Ion-induced atomic-like LMM and L^2MM Auger-electron emission from Mg, Al, Si, and Mg_xAl_{1-x}: Role of symmetric and asymmetric collisions

F. Xu, F. Ascione, N. Mandarino, P. Zoccali, P. Calaminici, A. Oliva, and A. Bonanno
Dipartimento di Fisica, Università della Calabria, 87036 Rende, Cosenza, Italy

N. Russo
Dipartimento di Chimica, Università della Calabria, 87036 Arcavacata di Rende, Cosenza, Italy
(Received 2 October 1992)

We present a detailed study on Auger-electron emission from sputtered light-target atomic species (Mg, Al, and Si) with one and two initial $2p$ core vacancies by low-energy (2–15 keV) noble-gas-ion bombardment on elemental and Mg_xAl_{1-x} alloy samples. We show that the Al atomic LMM peak shape varies sensitively with primary energy for Ar^+ but not for Ne^+, Kr^+, and Xe^+ projectiles, that the high-energy spectral regions of all three elements consist of many previously unresolved atomic line structures, and that the L^2MM-to-LMM intensity ratio depends on both primary ion energy and incidence angle. Adiabatic molecular-orbital correlation diagrams are also computed for describing the $2p$ core-electron promotion. Our results clearly show the differences in contributions of symmetric and asymmetric collisions to single and double inner-shell-electron excitation in different systems.

I. INTRODUCTION

Light-element L-shell Auger-electron emission induced by low-keV noble-gas-ion impact on solid surfaces has been the subject of intense studies for about two decades.[1,2] The spectra of Mg, Al, and Si are composed of many narrow lines attributed to atomic decays in vacuum and an underlying broad structure assigned to the deexcitation occurring inside the solid.[3–8] The $2p$ inner-electron excitation has been interpreted as due to radial couplings of the $4f\sigma$ molecular orbital within the framework of the electron promotion model.[9,10] Some computer simulation studies on the production of Al L-Auger electrons under Ar^+ ion bombardment have recently appeared in literature elucidating the physical mechanism of such interaction processes.[11–15]

Though the presence of small structures in the high-energy spectral region of all three elements has been noticed since the very early studies, relatively little attention has been paid to their nature and to their creation mechanism.[16–18] Benazeth, Benazeth, and Viel[19] and Thomas *et al.*[7,8] revealed two distinct features and assigned them to the atomic L^2MM and bulk L^2VV decays, respectively. The production of double $2p$ vacancy in these light elements is generally attributed to the projectile-target asymmetric collisions.[20–24]

On the other side, the single $2p$ vacancy in the target species can be created also in symmetric collisions. The threshold energy for encounters between the heavier projectile and lighter-target atoms is higher than that for those between two alike target atoms while the impact energy for the first projectile-target (p-t) encounter is larger than those in secondary target-target (t-t) cascade collisions. The relative contributions of symmetric and asymmetric encounters to the excitation events and their depth distributions are thus not trivial at all. Understanding of these aspects is of fundamental importance in studies of ion-induced Auger-electron emission.

In this paper we present a detailed systematic study on the LMM and L^2MM Auger features of Mg, Al, and Si produced by low-energy (2–15 keV) noble-gas-ion bombardment. We show that the high-energy regions of their derivative spectra are much more structured than previously reported ones. A careful analysis of these spectra taken at different incidence and detection angles indicates that all these features are of atomic nature and that such double inner electron promotion is caused by p-t collisions. For Ar^+ impact on Mg_xAl_{1-x} alloy samples the Mg-Al collisions are found to be the main mechanism for Mg L^2 excitation. The changes of the peak widths of Al LMM features as a function of the sample composition and the dependence of the Auger line shape on the projectile nature and on the primary energy provide further interesting insight into the relative importance of the symmetric and asymmetric collisions to the atomic L-shell Auger-electron emission from the target. Adiabatic molecular-orbital correlation diagrams are also computed for describing the $2p$ core-electron excitation in different collision systems.

II. EXPERIMENT AND CALCULATION METHODS

The experiments were conducted in an UHV chamber with a base pressure in the mid 10^{-10} Torr range. Samples were mechanically polished and cleaned *in situ* by ion bombardment. Good homogeneity of alloy samples was confirmed by scanning electron microscopy measurements. The surface Al concentration after prolonged sputtering was found to be 0.80, 0.56, and 0.31 for samples with nominal composition of 0.75, 0.50, and 0.25, respectively, nearly independent on the primary energy.

Noble-gas ions were produced by a differentially

pumped Atomika A-DIDA sputter gun with an energy between 2 and 15 keV. The ion discharge voltage was kept below 50 V to ensure a small doubly charged ion contamination (less than 3% for Ar^+) in the primary beam which was not mass analyzed. The ion incidence angle could be changed by rotating the sample manipulator. In addition, electrons with energy of 1.5 keV were also used as an excitation source for comparative studies. The gun was fixed at 40° relative to the ion beam and operated in a constant current mode. Only a trace of carbon but no oxygen was found on the sample surfaces.

Emitted electrons were detected either by a hemispherical energy analyzer (HEA) having a large acceptance angle of 50° and situated at 70° (30°) relative to the ion (electron) beam direction or by another hemispherical analyzer mounted on a rotatable goniometer (GHEA) with an acceptance angle of ~2°. Both analyzers laid in the plane determined by the incidence direction and the surface normal and were operated in the constant pass energy mode (100 eV for GHEA and 50 eV for HEA). For derivative spectra recorded with HEA a peak-to-peak modulation voltage of 1.25 V was applied.

The molecular-orbital correlation diagrams for various symmetric and asymmetric collision systems have been computed by using the linear combination of Gaussian-type orbital nonlocal density approximation (LCGTO-NLDA), a density-functional-like method successfully employed in theoretical studies of many chemical and physical processes. The details of this calculation method have been described elsewhere.[25,26]

The Kohn-Sham equations were solved by using the Vosko-Wilk-Nusair potential[27] and the effects of the nonlocal corrections were taken into account by employing the Perdew[28] and Perdew and Wang[29] functionals for the exchange and correlation energies, respectively. The orbital wave functions were expanded in basic functions of Gaussian type.[30] An auxiliary basis set was used to fit the correlation and exchange energies. The details of these basis sets for different atoms are given in Table I where we adopted the notation of Huzinaga[30] for orbital basis and used $(K_s,K_{spd};l_s,l_{spd})$ for auxiliary basis denoting with K_s (l_s) and K_{spd} (l_{spd}) the number of s-type Gaussians in the charge-density (exchange-correlation) basis and the number of s-, p-, and d-type Gaussians constrained to have the exponent in these bases, respectively. The adiabatic correlation diagrams have been performed on the neutral systems because it was demonstrated that, as far as the core-electron promotion is concerned, they are practically the same as those for ion-atom systems.[10]

TABLE I. Basis sets used in the calculation of the correlation diagrams.

Element	Orbital basis[a]	Auxiliary basis
Ne	(621/41/1*)	(4,4;4,4)
Mg	(6 321/411*/1)	(5,4;5,4)
Al	(7 321/621/1*)	(5,4;5,4)
Si	(7 321/621/1*)	(5,4;5,4)
Ar	(7 321/621/1*)	(5,4;5,4)
Ca	(6 3321/5 211*/1)	(5,5;5,5)
Mn	(6 3321/5 221*/41$^+$)	(5,5;5,5)
Ga	(6 3321/5 321*/41$^+$)	(5,5;5,5)
Zn	(6 3321/5 211*/41$^+$)	(5,5;5,5)
Ge	(6 3321/5 321*/41$^+$)	(5,5;5,5)
Kr	(6 3321/5 321*/41$^+$)	(5,5;5,5)
In	(6 3321/5 3321*/41$^+$)	(5,5;5,5)

[a]The * indicates the polarization functions and + the diffuse functions.

III. RESULTS AND DISCUSSIONS

In Figs. 1 and 2 we present the computed correlation diagrams which connect the united (internuclear distance $R=0$) and separated ($R=\infty$) atoms with molecular-orbital (MO) energy levels for symmetric (Mg-Mg, Al-Al, and Si-Si) and asymmetric (Ar-Mg, Ar-Al, Ar-Si, and Al-Mg) collision systems, respectively. To test our LCGTO-NLDA method, we have first calculated the correlation diagrams for two well-studied systems Ne-Ne

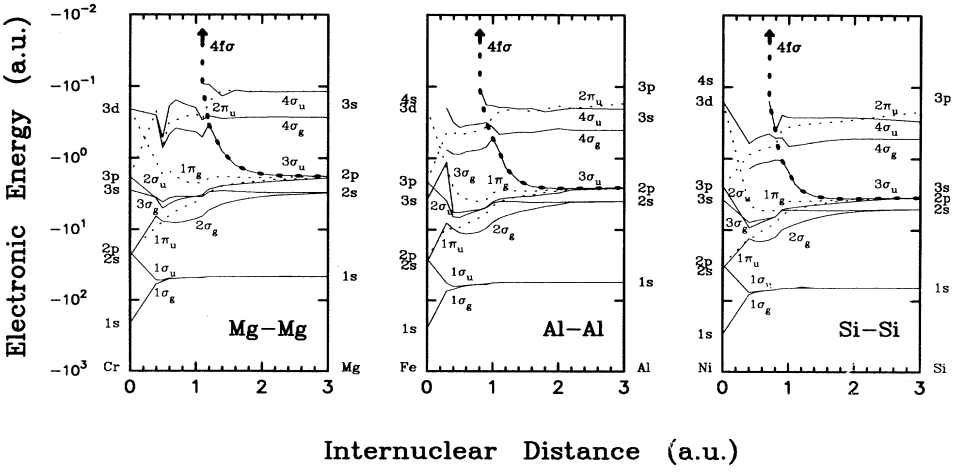

FIG. 1. Adiabatic molecular-orbital correlation diagrams for symmetric Mg-Mg, Al-Al, and Si-Si systems calculated with the LCGTO-NLDA method. Solid (dashed) curves denote σ (π) orbitals. The diabatization (thick dashed lines) was obtained by ignoring the screening gaps in the close avoided crossings. Both energy and internuclear distance are expressed in atomic units.

and Ar-Si. Comparison with the results obtained with the variable-screening model[31,32] shows very good agreement.

Since the early stage of the development of the molecular-orbital promotion model, this kind of correlation diagram has been widely used for describing the excitation of inner-shell electrons in slow ion-atom collisions.[9,10] The diabatization of the adiabatic MO curves is roughly approximated by ignoring the screening gaps at close avoided crossings, as the thick dashed lines drawn in Figs. 1 and 2. As two colliding atoms approach close to each other they transiently form a quasimolecule and the binding energies of some MO's are rapidly lowered and become comparable to the collisional energy broadening so that the electrons originally present in these orbitals can be promoted into the continuum. A simple step function of the internuclear distance is usually employed for describing the excitation probability[33] and will be adopted here for our qualitative discussions.

The results of Fig. 1 clearly show that the $2p$ electrons in symmetric collisions can be promoted from the $4f\sigma$ orbital (in the diabatic notation) through radial couplings. The internuclear distance $R^c_{\min}$ at which the promotion occurs is about 0.58 ± 0.03 Å for Mg-Mg, 0.42 ± 0.03 Å for Al-Al, and 0.37 ± 0.03 Å for Si-Si where the errors roughly estimate the uncertainties introduced in the diabatization process. These $R^c_{\min}$ values correspond to excitation energies of 1.1 ± 0.1, 1.7 ± 0.2, and 2.6 ± 0.3 keV, respectively. For asymmetric collisions, Fig. 2 indicates that L-shell-electron promotion occurs only in the lighter partner through $4f\sigma$ molecular-orbital curve crossings and that in collisions with Ar, $R^c_{\min}$ decreases with increase of the Z value. For core excitation in Mg, the threshold energy grows from Mg-Mg to Mg-Al, and to Mg-Ar.

In Fig. 3, we present three sets of detection-angle-resolved and peak-height-normalized doubly core excited L^2MM Auger-electron spectra obtained by 15-keV Ar^+-ion bombardment at $\theta_i = 40°$ from the surface normal on Mg, Al, and Si targets. These peaks are commonly attributed to autoionization transitions from an initial state with two $2p$ holes and an electron added in the outer $3p$ shell.[7,8] To better discern the other small structures, in Fig. 4 are shown the derivative spectra with 13-keV Ar^+-ion impact on Mg, Al, and Si in different experimental geometries. The bottommost curves are those for 1.5-keV electron stimulation. All the spectra are normalized to the height of the main *LMM* peaks and features in

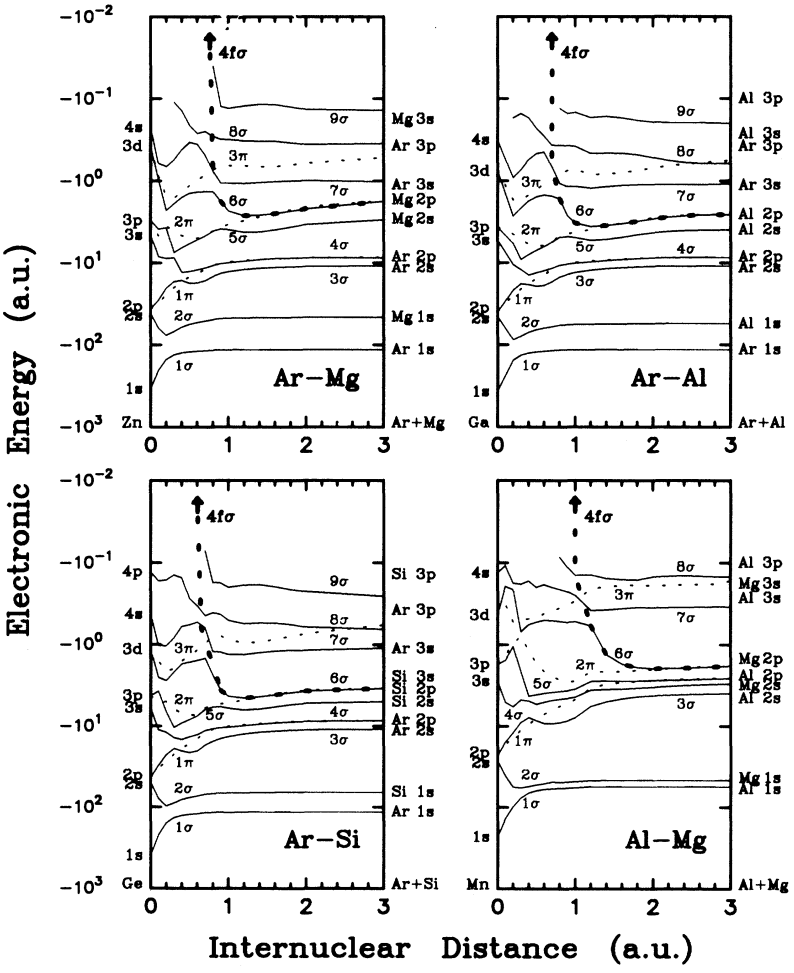

FIG. 2. Adiabatic molecular-orbital correlation diagrams for asymmetric Ar-Mg, Ar-Al, Ar-Si, and Al-Mg systems. For further explanation see caption of Fig. 1.

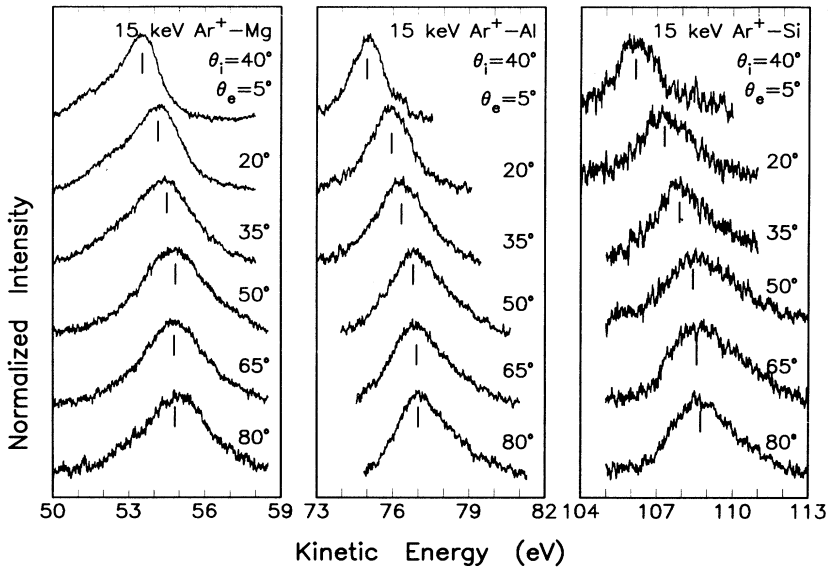

FIG. 3. Angle-resolved and secondary electron background subtracted Mg, Al, and Si main L^2MM Auger spectra for 15-keV Ar^+ impact. The spectra have been normalized to the same height. All the angles are relative to the surface normal.

the high-energy regions are magnified.

The electron impact does induce double L-shell-electron excitation in all these light element solids. Indeed, the L^2VV Auger decay involving two valence electrons can be clearly identified at 58.4±0.2, 82.8±0.3, and 105.7±0.5 eV for Mg, Al, and Si, respectively (energies are of the negative cursors and errors are the statistical uncertainties). The widths of these bulklike features, measured as the separation between the maximum and the minimum, range from 3.1±0.4 eV for Mg to 3.7±0.6 eV for Al and to 5.5±1 eV for Si.

The high-energy regions of Ar^+ excited spectra of all three elements present many structures. Some of them have been observed in our previous studies but many others have not been resolved.[6,24,34] The most pronounced peaks (labeled A) correspond to the ones shown in Fig. 3. All the other less intense peaks have linewidths (1.6±0.3 eV) much smaller than those of the corresponding L^2VV features and their energy positions differ quite a lot from that for electron stimulation and exhibit clear Doppler shifts as incidence and detection angles are varied, unambiguously indicating that Auger decays take place in the vacuum.

According to the MO model, a double $2p$ vacancy can be produced only in asymmetric collisions since in encounters between two alike atoms the core vacancies will be equally shared by the colliding partners. This has been confirmed in our previous experiments in which we observed a very strong dependence of Al L^2MM Auger yield on the projectile nature.[24]

The lack of a bulk feature thus suggests that the target atoms doubly inner excited in p-t collisions and not directly ejected in the vacuum would most probability transfer one of their vacancies to other target atoms in the subsequent collisions before they could nonradiatively deexcite in the solid.[24] As a consequence, nearly all the

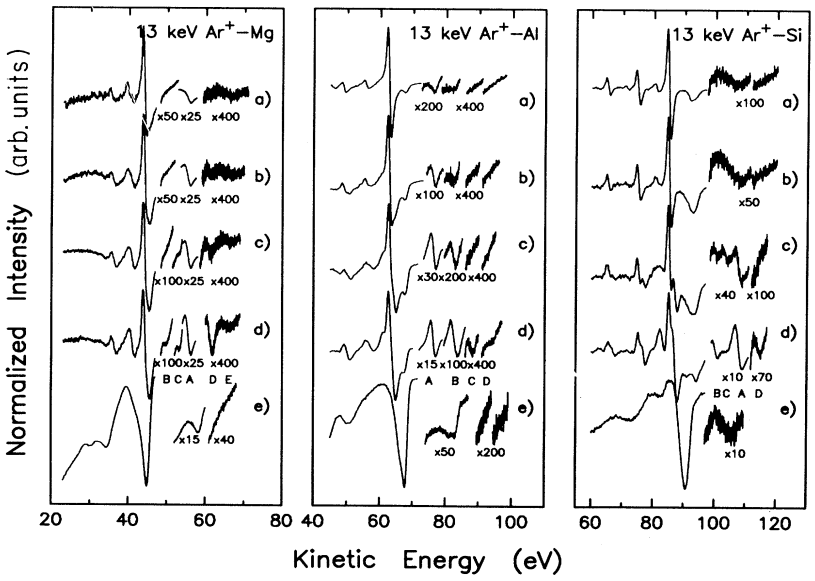

FIG. 4. Mg, Al, and Si Auger-electron derivative spectra taken with 13-keV Ar^+-ion bombardment (curves a–d) and with 1.5-keV electron stimulation (curve e). The experimental geometries are $\theta_i=0°$ and $\theta_e=70°$ (curve a); $\theta_i=20°$ and $\theta_e=50°$ (curve b); $\theta_i=40°$ and $\theta_e=30°$ (curve c); $\theta_i=70°$ and $\theta_e=0°$ (curve d); and $\theta_i=30°$ and $\theta_e=0°$ (curve e).

doubly excited atoms whose Auger electrons contributing to our L^2MM spectra originate from collisions occurring at the surface. For both Al and Si, the L^2MM intensity reduces greatly as the incidence angle gets closer to the surface normal, further indicating that most excitation events take place in the primary encounters and as the cascade develops only few collisions are still energetic enough to produce such excitation at surface. The relatively lesser attenuation of the Mg signal at normal incidence ($\sim 15\%$ of that at $\theta_i = 45°$) suggests, instead, a considerable contribution from secondary asymmetric collisions as well.

In the molecular-orbital electron promotion model, the creation of a double core vacancy requires that the two colliding partners reach a minimal approach distance smaller than $R^c_{\min}$. This also means the existence of a minimal transferred kinetic energy E^c_{trans} and of a critical scattering angle θ^c_{scatt}. Because of the rapid decrease of the cross section at small impact parameters, most observed excitation events occur at threshold values and the maximum Doppler shift should be observed at an angle θ^c_e corresponding to θ^c_{scatt}. The results of Fig. 3 show that for a fixed primary energy and a fixed incidence angle the Doppler shift and θ^c_e are smallest for Mg and largest for Si, indicating that $R^c_{\min}$ is smaller in Ar-Si than in Ar-Al and in Ar-Mg, in agreement with the correlation diagrams and with the fact that for normal Ar^+ incidence the L^2MM signals can be observed only for Mg but not for Al and Si.

The total L^2MM intensities for Mg, Al, and Si for $\theta_i = 45°$ are shown in the upper panel of Fig. 5. In the case of Mg, we also present the results for normal incidence. Before peak areas were calculated all spectra had been corrected for the analyzer transmission factor and background subtracted. For comparison, we also plot the total intensity of the atomic *LMM* features (lower panel of Fig. 5) obtained by subtracting the *LVV* contribution which was assumed to have the same spectral shape as that for electron stimulation.

Because of their atomic nature, the *LMM* and L^2MM intensities are nearly independent on the detection angle θ_e (the effects of anisotropic emission in the laboratory system are quite small for large analyzer acceptance angle) so the measured peak area should be directly proportional to the total atomic Auger yield. The results of Fig. 5 then indicate that such yields increase with the primary ion energy E_p and decrease with the atomic number of the interested element, consistent with the fact that the excitation threshold energies E^c_p for both asymmetric collisions (with Ar) and symmetric collisions increase with the target Z value. However, their growth rates versus E_p differ considerably as can be directly inferred from the L^2MM to *LMM* intensity ratio ρ, plotted in Fig. 6.

Since the double inner vacancy can be created only in asymmetric collisions while the single-core-electron excitation can result from cascade symmetric collisions as well and the ratio of probabilities for double and single $2p$ electron excitation in a given asymmetric collision is constant, the strong primary energy and incidence angle

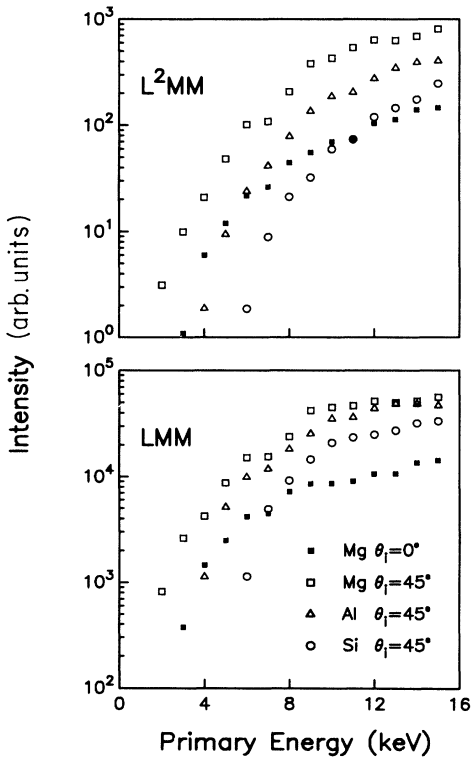

FIG. 5. Total intensity of L^2MM (upper panel) and *LMM* (lower panel) Auger signals for Mg, Al, and Si as a function of the Ar^+ primary energy for $\theta_i = 45°$ and $\theta_e = 25°$. For Mg, results for $\theta_i = 0°$ and $\theta_e = 70°$ are also shown. The experimental relative errors are 30% and 15% for L^2MM and *LMM* intensities, respectively.

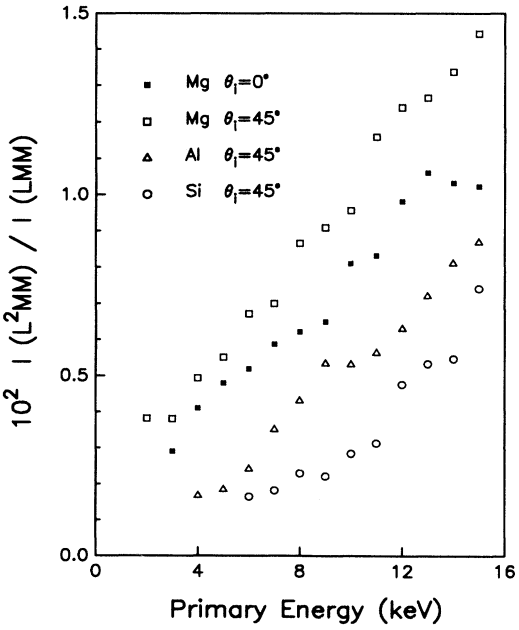

FIG. 6. Intensity ratio between the L^2MM and *LMM* atomic features vs the primary energy for Mg, Al, and Si under Ar^+-ion bombardment. The relative errors are 50%.

dependence of the intensity ratio between the L^2MM and LMM Auger signals (Figs. 4 and 6) suggests that the p-t collisions become increasingly important relative to the t-t ones for atomic LMM transitions as E_p increases and/or θ_i changes from the surface normal to grazing.

On the other hand, it is expected that the inner excitation in a given element should also depend on the collision partner. Results for Al showed that Ne projectiles do not cause double inner electron promotion while the L^2MM intensity for Ar impact is about 2 orders higher than that for Kr and 3 order higher than that for Xe.[24] To quantitatively evaluate this aspect for Mg in nearly symmetric collisions, we studied the intensity variation of the Mg L^2MM peak as a function of sample composition by bombarding Mg_xAl_{1-x} alloys. The partial overlap with one of the Al LMM feature, however, renders data analysis more laborious. In Fig. 7 are shown four sets of Al atomic Auger spectra for 2-, 8-, and 14-keV Ar^+ impact along normal and off-normal incidence angles for different Mg concentration.

We notice that both Al-I and Al-III peaks are gradually and rigidly shifted toward low kinetic energy as the Mg concentration C_{Mg} is increased, presumably because of a reduction in surface work function (4.28 eV for Al and 3.66 eV for Mg, Ref. 35). For $E_p=2$ keV, the Mg L^2MM peak appears at the low-energy side of Al-II in the emission from alloy samples, grows in relative intensity, and finally completely overlaps with and dominates on the Al contribution as C_{Mg} is increased. As the primary energy is raised, the increase of the Doppler shift and broadening renders the two peaks no longer separable.

It is important to point out that the intensity ratios between various Al peaks in Fig. 7 are independent both on sample composition and on Ar^+ primary energy, as do those between various Mg LMM features. We used the constant Al-II and Al-III intensity ratio for pure Al to subtract the Al-II contribution from the total peak area. The resulting Mg L^2MM intensity, normalized to the surface Mg concentration C_{Mg}, is plotted in Fig. 8 as a function of E_p for two different θ_i. It can be seen immediately that the Mg L^2MM yield is about an order of magnitude larger in alloy than in pure Mg and is an increasing function of the Al content, suggesting that the Al-Mg collisions greatly prevail on the Ar-Mg ones. Further, the slower growth rate of this intensity at the low E_p region for alloys than for pure Mg clearly indicates a lower threshold energy for Al-Mg than for Ar-Mg.

The spectra of Fig. 7 show that, for $E_p=2$ keV, the main Al atomic LMM peak is symmetric for both normal and off-normal Ar^+ incidence and its width remains independent on the sample composition. For $E_p=8$ and 14 keV and $\theta_i=0°$, a shoulder appears on the high-energy side and the overall linewidth increases with C_{Mg} in the alloys. This shoulder is mainly due to excitation in Ar-Al cascade collisions which are, on average, faster than those in Al-Al ones and its absence in the spectra for $E_p=2$ keV simply suggests that at such low E_p the Ar-Al

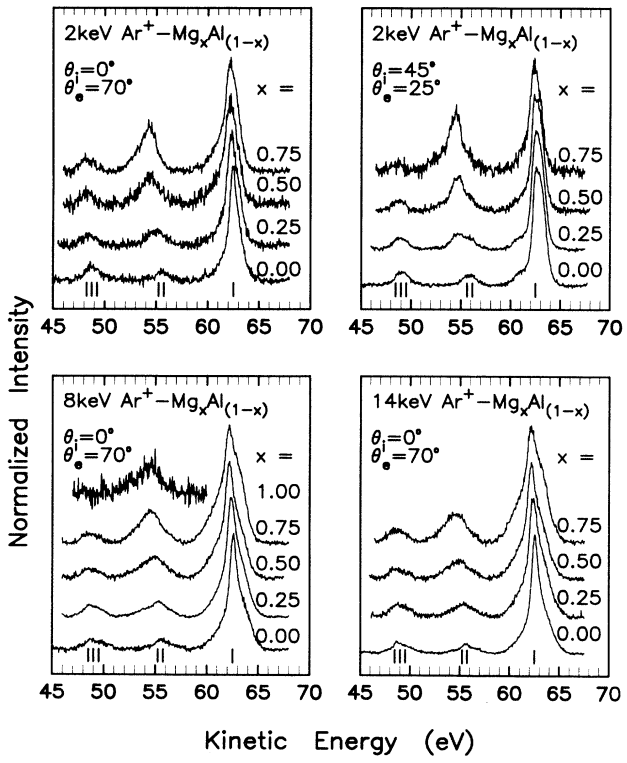

FIG. 7. Al LMM Auger-electron spectra for Ar^+-ion impact on Mg_xAl_{1-x} alloy samples. The feature at the low-energy side of the Al-II peak is due to the Mg L^2MM transition.

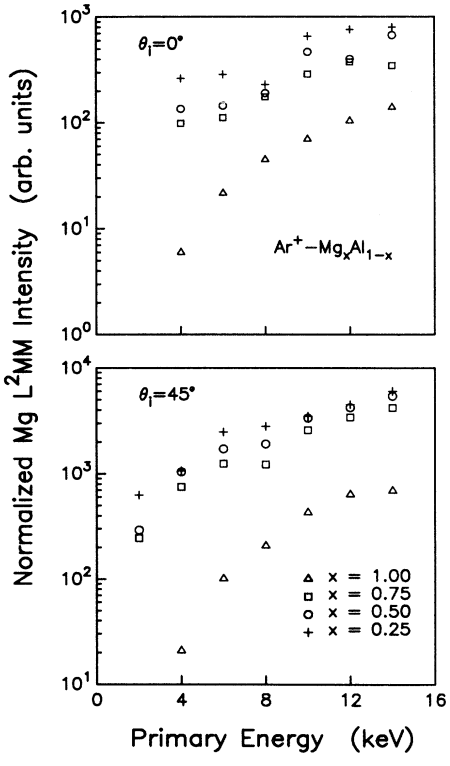

FIG. 8. Intensity of Mg L^2MM Auger electrons emitted from Mg_xAl_{1-x} alloys under Ar^+-ion bombardment as a function of E_p. All the values have been normalized to the Mg surface concentration. The typical errors are 30%.

encounters are not effective. We notice that for $E_p > 4$ keV its relative intensity increases gradually because of the increasing importance of asymmetric collisions. Indeed, for alloys samples, the relative weights of Ar-Al and Al-Al encounters in contributing to Al $2p$ excitation are linearly and quadratically proportional to C_{Al}, respectively. Given that the threshold transferred energy, E^c_{trans}, is higher for Ar-Al than for Al-Al, the Doppler shifts and broadening should be a decreasing function of C_{Al}.

In the upper panels of Fig. 9 we show detection-angle-resolved Auger spectra for Ne^+, Ar^+, Kr^+, and Xe^+ ion impact on an Al surface at $\theta_i = 40°$ for various energies. These spectra, relative to the main *LMM* transition in a neutral Al atom, do not show any noticeable change in line shape for Ne^+, Kr^+, and Xe^+ projectiles in the energy range 3–15 keV and is very similar to that for 5-keV Ar^+ bombardment, suggesting that in these cases the Al $2p$ excitation is essentially produced by Al-Al symmetric collisions. We attribute the high-energy shoulder to emission from fast moving Al atoms. Indeed, for off-normal incidence, many energetic Al atoms excited in the first few symmetric collisions have scattering angles large enough to escape from the surface without need of further collisions.

The spectra of the same transition peak obtained by Ar^+ impact at various primary energies along $\theta_i = 60°$ for three different observation angles are presented in the lower panels of Fig. 9. The peak shape changes greatly as E_p is increased and a new Doppler structure appears at energy 2–3 eV higher than the main one. We assign this feature to excitation in the primary Ar-Al encounters since the shift is very similar to that observed for the L^2MM peak, certainly due to primary asymmetric collisions. Further, the projectile energy at which the shoulder appears is greater than 4–5 keV where the Ar-Al contribution to Al $2p$ excitation becomes increasingly important. The position of this Doppler component shows clear dependence on θ_e but is relatively insensitive to E_p because most of the excited atoms have a velocity corresponding to the threshold value. Nevertheless, its relative intensity is strongly dependent on E_p and θ_i, consistent with the previous discussion on the L^2MM to *LMM* intensity ratio.

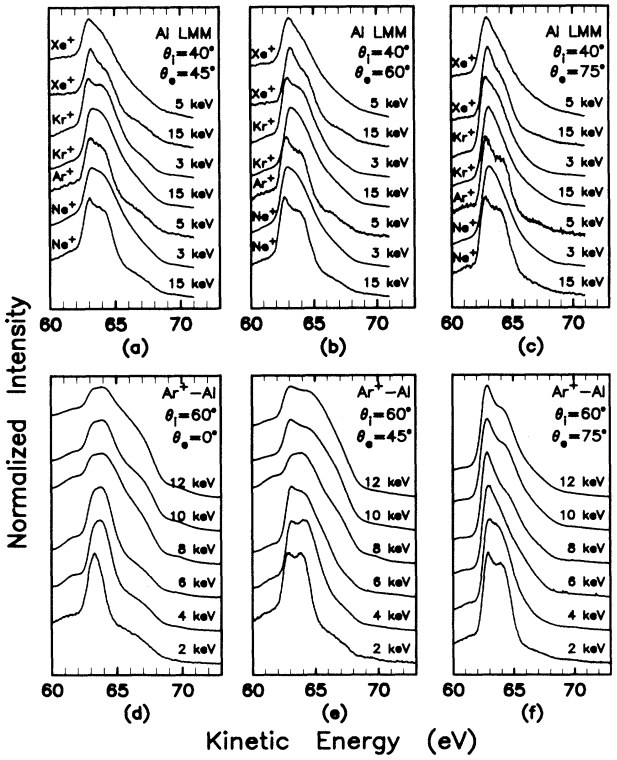

FIG. 9. Angle-resolved Al main *LMM* Auger peak for various projectile ions with different primary energies (a)–(c) and for Ar^+ impact with $2 \le E_p \le 12$ keV (d)–(f).

We point out that a quantitative estimate of the total asymmetric contribution to *LMM* Auger signals cannot be easily obtained from the intensity of the shifted component because Ar projectiles can excite Al atoms also in cascade collisions. Indeed, many of the target atoms excited in this way may be ejected without a well-defined direction, contributing only to the broadening of the main unshifted component. On the other hand, for off-normal incidence, symmetric collisions can also be responsible for the ejection of fast moving excited target particles producing a large shift, as seen in Fig. 9.

To get a better and quantitative understanding of the relative role played by the symmetric and asymmetric collisions in core excitation, in our opinion, many theoretical studies regarding the probability functions of collisional excitation, vacancy transfer, and collisional deexcitation processes should be performed and systematic computer simulation investigations should be carried out on different collision systems with different primary energies and different incidence angles. Such simulations should not be confined only to Auger yield but also be extended to the (angle-resolved) electron energy spectra since they can also provide a direct test on the spatial and velocity distribution of the sputtered excited particles.

IV. CONCLUSIONS

In conclusion, we have presented a study on Auger-electron spectra of Mg, Al, Si, and Mg_xAl_{1-x} alloys. Based on line-shape variation as a function of a set of experimental parameters, we showed that the relative contributions from symmetric and asymmetric collisions to core-electron excitation vary from one system to another and depend on the specific excitation event considered. The main results of this study can be summarized as follows.

(1) The double-core-electron excitation is produced by projectile-target asymmetric collisions while the single-core vacancy can be created in both asymmetric and symmetric encounters. The strong dependence of the L^2MM Auger signal and the L^2MM to *LMM* intensity ratio on the ion incidence angle clearly indicates that the *p-t* collisions mainly take place at the surface or in the near-surface region whereas the *t-t* ones can well develop deep in the bulk matrix.

(2) The threshold energy for excitation of the target atoms in asymmetric collisions with Ar is smallest for Mg and largest for Si and that for Mg $2p$ increases from Mg-Mg to Mg-Al, and to Mg-Ar, in agreement with the prediction of our calculated Mo correlation diagrams.

(3) Angle-resolved Al *LMM* Auger spectra show essentially no line-shape variation for Ne^+, Kr^+, and Xe^+ impact with energies of 3–15 keV indicating the predominance of the symmetric collisions. Large changes in peak shape for Ar^+-ion bombardment as a function of detection angle and of primary energy suggests a substantial contribution of the asymmetric p-t collisions for $E_p \geq 5$ keV.

ACKNOWLEDGMENTS

We thank V. Fabio and E. Li Preti for technical collaboration. The physics group is also affiliated to Consorzio Interuniversitario Nazionale per la Fisica della Materia. This work is partially supported by CNR under contract of "Progetto Finalizzato-Materiali Speciali per Tecnologie Avanzate."

[1]E. W. Thomas, Vacuum **34**, 1031 (1984).
[2]J. A. D. Matthew, Phys. Scr. T **6**, 79 (1983).
[3]G. Zampieri and R. Baragiola, Phys. Rev. B **29**, 1480 (1984).
[4]M. Nègre, J. Mischler, and N. Benazeth, Surf. Sci. **157**, 436 (1985).
[5]S. V. Pepper and P. R. Aron, Surf. Sci. **169**, 14 (1986).
[6]A. Bonanno, F. Xu, M. Camarca, R. Siciliano, and A. Oliva, Phys. Rev. B **41**, 12 590 (1990).
[7]W. A. Metz, K. O. Legg, and E. M. Thomas, J. Appl. Phys. **51**, 2888 (1980).
[8]R. Whaley and E. W. Thomas, J. Appl. Phys. **56**, 1505 (1984).
[9]U. Fano and W. Lichten, Phys. Rev. Lett. **14**, 627 (1965).
[10]M. Barat and W. Lichten, Phys. Rev. A **6**, 211 (1972).
[11]J. J. Vrakking and A. Kroes, Surf. Sci. **85**, 153 (1979).
[12]T. D. Andreadis, J. Fine, and J. A. D. Matthew, Nucl. Instrum. Methods **209/210**, 495 (1983).
[13]O. Grizzi and R. Baragiola, Phys. Rev. A **35**, 135 (1987).
[14]M. H. Shapiro and J. Fine, Nucl. Instrum. Methods B **44**, 43 (1989).
[15]M. Hou, C. Benazeth, P. Hecquet, and N. Benazeth, Nucl. Instrum. Methods B **48**, 625 (1990).
[16]J. Kempf and G. Kaus, Appl. Phys. **13**, 261 (1977).
[17]C. Benazeth, N. Benazeth, and L. Viel, Surf. Sci. **65**, 165 (1977).
[18]K. Wittmaack, Surf. Sci. **85**, 69 (1979).
[19]C. Benazeth, N. Benazeth, and L. Viel, Surf. Sci. **78**, 625 (1978).
[20]K. Wittmaack, Phys. Lett. **74A**, 197 (1979).
[21]P. Viaris de Lesegno and J. F. Hennequin, Surf. Sci. **103**, 257 (1981).
[22]J. F. Hennequin, R. L. Inglebert, and P. Viaris de Lesegno, Surf. Sci. **140**, 197 (1984).
[23]S. Valeri and R. Tonini, Surf. Sci. **220**, 407 (1989).
[24]F. Xu, M. Camarca, A. Oliva, N. Mandarino, P. Zoccali, and A. Bonanno, Surf. Sci. **247**, 13 (1991).
[25]*Metal-Ligant Interactions: From Atoms to Clusters, to Surfaces,* edited by D. R. Salahub and N. Russo (Kluwer, Dordrecht, 1992).
[26]*Density Functional Methods in Chemistry,* edited by J. Labanowsky and J. Andzelm (Springer-Verlag, New York, 1992).
[27]S. H. Vosko, L. Wilk, and M. Nusair, Can. J. Phys. **58**, 1200 (1980).
[28]J. P. Perdew, Phys. Rev. B **33**, 8822 (1986).
[29]J. P. Perdew and Y. Wang, Phys. Rev. B **33**, 8800 (1986).
[30]*Gaussian Basis Sets for Molecular Calculations,* edited by S. Huzinaga (Elsevier, Amsterdam, 1984).
[31]J. Eichler and U. Wille, Phys. Rev. Lett. **33**, 56 (1974).
[32]D. Schneider, G. Nolte, U. Wille, and N. Stolterfoht, Phys. Rev. A **28**, 161 (1983).
[33]R. K. Cacak, Q. C. Kessel, and M. E. Rudd, Phys. Rev. A **2**, 1327 (1970).
[34]A. Oliva, A. Bonanno, M. Camarca, and F. Xu, Nucl. Instrum. Methods B **58**, 333 (1991).
[35]*CRC Handbook of Physics and Chemistry,* 65th ed. (CRC, New York, 1985).